THE ASTROPHYSICAL JOURNAL, 468:907–920, 1996 September 10

HOT MAGNETIC FIBRILS: THE SLOW CONTINUUM REVISITED

R. KEPPENS[1]
Belgian National Fund of Scientific Research, Kiepenheuer-Institut für Sonnenphysik, Schöneckstrasse 6, D-79104 Freiburg, Germany
Received 1995 July 11; accepted 1996 March 25

ABSTRACT

We investigate the importance of the slow continuum (from linear, ideal magnetohydrodynamics [MHD]) for hot, evacuated, and strongly magnetic fibrils with nonnegligible radial structure. The radial structure allows for both slow and Alfvén resonant absorption of acoustic power (in linear, visco-resistive MHD). When calculating how efficiently the acoustic power is absorbed by such "hot magnetic fibrils," embedded in a uniform compressible medium, as a function of the *real* driving frequency, it is found that the axisymmetric component of the acoustic excitation is absorbed quite strongly for frequencies within the range of the slow continuum.

Additionally, for these one-dimensional hot magnetic fibrils, a sequence of absorption maxima accumulates in real driving frequency above the range of the slow continuum, still within the Alfvén continuum. The maximal absorption coefficients reach 80% and more. We identify the complex optimal driving frequencies and the associated complex leaky eigenmodes responsible for these absorption maxima.

The leaky eigenmodes relate to the well-known tube speed modes of a uniform, hot, and evacuated flux tube. The *complex* eigenfrequencies of the leaky eigenmodes of the radially structured fibrils are calculated from the impedance criterion that these eigenfrequencies satisfy.

We define the generally *complex* optimal driving frequencies to be those driving frequencies at which total (100%) absorption of the incoming wave field takes place. They also obey an impedance criterion, similar to the one that defines the eigenfrequencies. Both impedance criteria demonstrate clearly the connection between optimal driving frequencies and leaky eigenmodes. This also calls for a reevaluation of the results of Goossens & Hollweg, in which optimal and total resonant absorption for *real* driving frequencies and the *complex* leaky eigenmodes was discussed.

For network and plage magnetic elements in the solar atmosphere, our results may be relevant for wave interactions within a layer situated at a geometrical height of about 400 km above photospheric $\tau = 1$.

Subject headings: MHD — Sun: magnetic fields

1. INTRODUCTION

In ideal magnetohydrodynamics (MHD), an equilibrium gradient across otherwise straight magnetic field lines introduces continuous ranges of equilibrium frequencies, commonly known as the Alfvén and slow continuum (see, e.g., Goedbloed 1983). Assuming an ignorable vertical (field-aligned) coordinate z, and Fourier-analyzing as $\exp(ik_\parallel z)$, the (squared) Alfvén frequencies are given by

$$k_\parallel^2 B_z^2/(\mu\rho) \equiv k_\parallel^2 v_A^2 ,$$

and the (squared) slow frequencies are given by

$$k_\parallel^2 B_z^2 c^2/[\mu\rho(c^2 + v_A^2)] \equiv k_\parallel^2 c_T^2 .$$

In these expressions, B_z denotes the (vertical) magnetic field, ρ is the density, and μ is the magnetic permeability. From these, the squared Alfvén speed is introduced as $v_A^2 = B_z^2/(\mu\rho)$, while c^2 denotes the squared sound speed and c_T^2 is the squared tube speed. It is the aim of this paper to illustrate how *both* continua allow for efficient absorption of acoustic power by hot magnetic (straight) fibrils with internal radial structure (one dimension), due to resonant absorption.

Resonant absorption has been studied extensively in the context of linear MHD: in essence, due to the equilibrium gradient across the field lines in a one-dimensional magnetic fibril, it becomes possible to excite resonantly a single flux surface at one of its natural frequencies (slow or Alfvén). Any usually ignorable dissipative mechanism prevents the development of infinite gradients in the disturbances by the introduction of a dissipative layer of small, finite width about the critical surface. Within the framework of linear dissipative MHD, one has analytic information about the extent of this dissipative layer and the actual variation of the linear disturbances within it (Goossens, Ruderman, & Hollweg 1995). The total power extracted from the excitation due to such "resonant absorption" can hence be determined by (i) solving for the linear disturbances outside the dissipative layer using ideal MHD, (ii) incorporating the linear analytic (!) dissipative MHD results to deal with the resonance, and (iii) comparing the radially incoming versus radially outgoing energy fluxes. Indeed, the net effect of each resonant layer in which dissipation occurs is to extract some of the incoming acoustic power and heat up the plasma locally.

Resonant absorption due to the Alfvén continuum received most attention in the literature, in particular within the context of coronal loop heating mechanisms and p-mode absorption by sunspots (see, e.g., Hollweg 1988; Lou 1990; Poedts, Goossens, & Kerner 1989, 1990; Goossens & Poedts 1992). In both cases, the power carried by waves exciting the magnetic structure is partly scattered and partly transmitted, and part of the transmitted power may be dissipated into heat due to resonant absorption.

[1] On leave from Center for Plasma-Astrophysics, K. U. Leuven, Belgium. Presently at FOM Institute for Plasma Physics, Rijnhuizen, P.O. Box 1207, 3430 BE Nieuwegein, Netherlands.

Naturally, in order for such dissipation to occur, it is required that the frequency spectrum of the exciting waves overlaps with the Alfvén and/or slow frequency spectrum of the excited equilibrium structure. In the simplest model of a flux tube embedded in homogeneous unmagnetized surroundings characterized by a sound speed c, the frequencies ω of the exciting acoustic waves all satisfy $\omega > k_{\|} c$, and the low-frequency slow continuum usually cannot be accessed. Therefore, most studies focused on Alfvén resonant absorption. However, there are two cases of physical interest in which a study of *slow* resonant absorption in one-dimensional magnetic flux tubes deserves particular attention. First, *hot and evacuated magnetic flux tubes* may have internal tube speeds c_T in excess of the external sound speed c, such that the slow continuum is (partly) accessible for acoustic excitation. Second, in *twisted magnetic flux tubes*, the degeneracy of the frequency ranges of Alfvén and slow continuum with respect to the azimuthal variation is lifted, and slow resonant absorption cannot a priori be ignored. In this paper, we discuss the former case of hot and evacuated, but untwisted, flux tubes. Our aim is to investigate and compare the efficiency of resonant absorption within *both* the slow and the Alfvén continuum.

A prerequisite for interpreting the efficiency of resonant absorption in magnetic fibrils is a full understanding of the linear MHD spectrum of the combined system consisting of the fibril and its (here, assumed uniform and unmagnetized) surroundings (Goossens & Hollweg 1993). In particular, as frequencies of interest for acoustic wave excitation satisfy $\omega > k_{\|} c$, the eigenfrequencies of *leaky* modes must be calculated, and their influence on the absorption efficiency must be established. The term "leaky" refers to the fact that for real $k_{\|}$, eigenmodes of the fibril plus its (infinite!) surroundings have complex eigenfrequencies $\omega \equiv \omega_R + i\omega_I$ when their real part $\omega_R > k_{\|} c$, since the mode will be damped due to acoustic wave leakage into the surroundings (for results on leaky modes of uniform flux tubes, see Wilson 1981; Spruit 1982; Cally 1986). In cases of interest here, the real part ω_R can lie within either the slow or the Alfvén continuum (or both), so that in such cases, the damping ω_I has a contribution from the resonant absorption internal to the fibril. Although a connection between efficient resonant absorption and leaky eigenmodes was anticipated (Goossens & Hollweg 1993), the actual calculation of the complex eigenfrequencies for a one-dimensional magnetic flux tube embedded in uniform (wave carrying) surroundings awaited the realization that all eigenfrequencies (leaky and nonleaky alike) satisfy an impedance matching (Keppens 1995a, 1995b). In the Appendix, we provide details about the basic ideas that have led to this realization. In essence, the important linear quantities are the (total) linear pressure δP and the velocity component normal to the flux tube boundary, δv_R (the subscript R refers to the radial direction, which is the normal for a cylindrical flux tube), and their ratio defines the normal acoustic impedance $Z \equiv \delta P/\delta v_R$ (usually made dimensionless, or "specific" by division through ρc; see, e.g., Morse & Feshbach 1953). When we decompose the wave field external to the flux tube into the exciting (subscript "exc") and the scattered (subscript "sc") part (that part that is due entirely to the presence of the flux tube), we may define an impedance for each of these wave fields separately. Hence, by denoting the internal wave field as transmitted (subscript "tr"), we have three impedances: the transmitted one $Z_T \equiv \delta P_{\rm tr}/\delta v_{R,\,tr}$, the exciting[2] one $Z_E \equiv \delta p_{\rm exc}/\delta v_{R,\,\rm exc}$, and the scattered one $Z_S \equiv \delta p_{\rm sc}/\delta v_{R,\,\rm sc}$. Note that we use total linear pressure δP for the transmitted wave field, while in the unmagnetized surroundings, the external linear pressure perturbation is made up of the linear gas pressure δp alone. In contrast to this decomposition of the external wave field into its exciting and scattered part, we may prefer to take the geometry of the flux tube into account and decompose the external wave field into radially incoming and outgoing cylindrical waves instead (see Appendix), so that we may introduce incoming ($Z_I \equiv \delta p_{\rm in}/\delta v_{R,\,\rm in}$) and outgoing ($Z_O \equiv \delta p_{\rm out}/\delta v_{R,\,\rm out}$) impedances as well. Since the total pressure perturbation and the normal velocity component are continuous across the flux-tube boundary, we then have several ways to calculate the transmitted normal acoustic impedance, namely,

$$Z_T = \frac{\delta P_{\rm tr}}{\delta v_{R,\rm tr}} = \frac{\delta p_{\rm exc} + \delta p_{\rm sc}}{\delta v_{R,\rm exc} + \delta v_{R,\rm sc}} = \frac{\delta p_{\rm in} + \delta p_{\rm out}}{\delta v_{R,\rm in} + \delta v_{R,\rm out}} . \quad (1)$$

These equalities can be manipulated to yield

$$\frac{\delta v_{R,\rm sc}}{\delta v_{R,\rm exc}} = \left(\frac{Z_T - Z_E}{Z_S - Z_T}\right), \quad (2)$$

and also

$$\frac{\delta v_{R,\rm out}}{\delta v_{R,\rm in}} = \left(\frac{Z_T - Z_I}{Z_O - Z_T}\right). \quad (3)$$

A careful examination of these expressions reveals that the left-hand sides are proportionate to the relative phase shift and amplitude modifications suffered by the exciting wave field to yield the scattered wave (eq. [2]), and similarly for the incoming wave field to yield the outgoing wave[3] (eq. [3]). Yet, other manipulations can give information on the transmitted wave field with respect to either the exciting or the incoming wave field. Two important conclusions can be drawn from equations (2) and (3):

1. No incoming (or no exciting) wave corresponds to the impedance criterion $Z_O = Z_T$ (or $Z_S = Z_T$). This impedance criterion can thus be used to calculate the eigenfrequencies of the eigenmodes of the cylindrical scatterer embedded in its infinite and wave-carrying surroundings (see also Keppens 1995a, 1995b). Those eigenfrequencies ω that have their real part ω_R in excess of $k_{\|} c$ lead to acoustic wave leakage into the surroundings and are referred to as "leaky" eigenmodes, while those with $\omega_R \leq k_{\|} c$ are termed "nonleaky."

2. 100% absorption, or no outgoing wave, corresponds to the impedance criterion given by $Z_I = Z_T$. This impedance criterion defines the (complex) optimal driving frequencies. Hence, we define an optimal driving frequency from the condition that when one drives the system at this (complex) frequency, an analysis of the external wave field into incoming and outgoing waves leads to a zero ampli-

[2] In Keppens (1995b), this was $Z_E \equiv \delta p_{\rm exc}/(-\delta v_{R,\rm exc})$. In this paper, we drop this extra minus sign.

[3] These expressions are related to the so-called T-matrix and S-matrix of a cylindrical scatterer; see Appendix. Keppens (1995b) uses eq. (2) to calculate the components of the T-matrix for a flux tube with a thin transition layer analytically. The components of both matrices for cylindrical scatters are related by $S = 1 - 2T$.

tude for the outgoing wave, such that one may say that the incoming wave is totally absorbed by the scattering object. From equation (3), this is equivalent to the impedance criterion $Z_I = Z_T$.

What exactly these impedance criteria mean for our one-dimensional magnetic flux fibril will be explained in more detail in this paper. Suffice it to say that they will allow us to give, for the first time, a complete and detailed account of the connection between efficient resonant absorption and leaky eigenmodes. Therefore, these results support and supplement the results of Goossens & Hollweg (1993), in which this connection was first realized.

As we restrict ourselves in this paper to study hot magnetic fibrils with nonnegligible internal radial structure, we expect to find leaky modes, satisfying $Z_S = Z_T$, in relation with the slow continuum since it is derived from the radial variation of the tube speed. This is because, as is well known, the tube speed c_T in a thin, but uniform, flux tube plays the role of an accumulation point (in longitudinal phase speed $\omega/k_\parallel$) of infinitely many discrete eigenmodes (Defouw 1976). However, it is not immediately obvious how these discrete modes behave when the single slow frequency of the uniform flux tube is replaced (or "smeared out") in a slow continuum. As mentioned above, the impedance criterion that the eigenfrequencies satisfy will allow us to address the faith of these modes. We will show the following:

1. That sequences of leaky modes (for which $Z_S = Z_T$) are found to accumulate in (the real part of the) frequency toward the maximum in the slow continuum;
2. That associated optimal, but in general complex, frequencies for which $Z_I = Z_T$ exist at which 100% absorption occurs.

We investigate how the (complex) leaky modes and the (mostly complex) optimal driving frequencies play a role in the acoustic excitation of a hot magnetic fibril with *real driving frequency*. This will call for a reevaluation of the results of Goossens & Hollweg (1993).

Finally, within the solar context, the thin hot magnetic fibrils studied in this paper are (admittedly poor) representations for the omnipresent magnetic elements of strong (kG) fields and positive temperature contrast (see, e.g., Keller 1992; Schüssler 1991; Solanki 1993). As these are embedded in almost field-free, convective surroundings, the scattering and absorption processes we are dealing with here within the framework of linear MHD may serve to understand better the more realistic dynamic situation. When we crudely ignore the dynamic nature of solar magnetic elements (as evidenced by the numerical simulations of Steiner et al. 1996) and compare the semiempirically determined vertical structure of plage and network small-scale magnetic fluxtubes (from Keller et al., 1990) with our (one-dimensional) model parameters, we can identify a layer at approximately 400 km geometrical height above the photospheric $\tau = 1$ level at which slow resonant absorption, and the leaky modes accumulating toward the slow continuum, may play a role in wave interactions with magnetic elements.

The paper is organized as follows. For a particular equilibrium configuration modeling a hot magnetic fibril, we give a rather detailed account of its absorption properties due to slow and Alfvén resonant absorption, and we clarify the connection with leaky modes and optimal driving frequencies. This is done in § 2. We calculate exact eigenfrequencies and optimal driving frequencies using the impedance criteria given above. In § 3, we illustrate the effects of varying the evacuation, the radial stratification, and the thickness of the hot magnetic fibril equilibrium, and we discuss its relevance to solar magnetic elements. We conclude in § 4.

2. LINEAR ANALYSIS OF A ONE-DIMENSIONAL HOT FIBRIL

2.1. *The One-dimensional Fibril Equilibrium*

The ideal, axisymmetric one-dimensional MHD equilibrium that we use to model a straight magnetic fibril with internal radial structure is adopted from Lou (1990). This equilibrium had the practical "sharpness" parameter λ, which controlled the sharpness of the transition between the magnetized and the external unmagnetized region. We define a generalized Lou-type equilibrium as characterized by two physical parameters, λ and D. The parameter λ still has the interpretation of a sharpness parameter, while D measures the density ratio between the external and the axial density $D = \rho_0/\rho_1(0)$ (from here on, a subscript "0" refers to external quantities, while a subscript "1" refers to internal quantities). If we scale the equilibrium quantities (and denote scaled quantities by a superscript "*") to the cylinder radius a, the total axial field strength $B_1(0)$, and the axial density $\rho_1(0)$, the defining equation (for radial coordinate $0 \le R \le 1$) is

$$p_1^*(R) = \frac{p_{\rm ext}}{3}(1 + e^{-\lambda(R-1)^2})(1 + 0.5e^{-\lambda(R-1)^2}) . \quad (4)$$

The density profile can be chosen independently, but to keep the physical meaning of λ as a sharpness parameter, we proceed as follows. If we introduce the factor A as

$$A = \frac{1 - D}{De^{-\lambda} - 1} , \quad (5)$$

we can define a Lou-type density profile as

$$\rho_1^*(R) = \frac{1 + Ae^{-\lambda(R-1)^2}}{1 + Ae^{-\lambda}} . \quad (6)$$

We note that in the orginal equilibrium used by Lou (1990), the factor A was equal to one, such that the actual density contrast D was limited to small values ($D \le 2$), through its nontrivial dependence on the sharpness parameter λ. The (vertical) magnetic field $B_{z1}^*(R)$ is then determined from the static equilibrium condition and varies smoothly from its axial value $B_{z1}^*(0) = 1$ to zero at the flux-tube radius. In these equations, the parameter $p_{\rm ext} \equiv p_1^*(1)$ measures the dimensionless pressure at the flux-tube radius and relates to the external pressure p_0 as $p_0 = p_{\rm ext}[B_1(0)]^2/2\mu$. As noted previously by Goossens & Poedts (1992), the parameter $p_{\rm ext}$ is actually dependent on the defining equilibrium parameter λ,

$$p_{\rm ext} = \frac{0.5}{[1 - (1 + e^{-\lambda})(1 + 0.5e^{-\lambda})/3]} . \quad (7)$$

Further, the external density $\rho_0 = \rho_1^*(1)\rho_1(0)$. Some other physical parameters that can be derived from λ, D, and the

(dependent) parameter $p_{\rm ext}$ are

$$\rho_1^*(1) = D\ ,$$
$$p_1^*(0) = \frac{p_{\rm ext}}{3}\,(1 + e^{-\lambda})(1 + 0.5e^{-\lambda})\ ,$$
$$\frac{v_{A1}(0)}{c_0} = \sqrt{\frac{\rho_1^*(1)}{\gamma p_{\rm ext}}}\ , \qquad (8)$$
$$\frac{c_1(0)}{c_0} = \sqrt{\gamma p_1^*(0)}\,\frac{v_{A1}(0)}{c_0}\ .$$

In this Lou-type equilibrium, large λ corresponds to an almost uniform untwisted flux tube with a thin transition layer. The ratio of specific heats is $\gamma = 5/3$, as usual.

2.2. *Slow and Alfvén Resonant Absorption*

In the remaining part of this section, we consider the particular case of a fibril with its thickness characterized by $k_\parallel a = 0.9$, sharpness $\lambda = 75$, and with a density contrast of $D = 5$. The radial variation of ρ_1^*, B_{z1}^*, and p_1^* is shown in Figure 1. We show also the variation of the Alfvén, tube, and sound speed across the fibril, normalized to the external sound speed c_0. We infer from these profiles that the temperature contrast is about $T_1 \approx 1.66T_0$ over 75% of the fibril radius a, and for typical photospheric pressures of the order of $p_0 = 10^4$ Pa, the field strength is roughly 1.8 kG over a similar radial extent. Hence, this particular hot magnetic fibril bears no immediate resemblance to a magnetic element (which has a lower temperature contrast), apart from its field strength. Variations in the equilibrium parameters (and in particular, parameter values more suitable for magnetic elements) will be considered in § 3.

Due to the variation of the equilibrium in the outer 25% of radius, we must integrate the Hain & Lüst (1958) equation that governs the linear disturbances about this axisymmetric one-dimensional, ideal MHD equilibrium. Omitting unduly details (which can be found, e.g., in Sakurai, Goossens, & Hollweg 1991a, their eqs. [9] and [10]), the linear ideal MHD equations can be reduced to a system of two linear first-order ordinary differential equations in the variables $(\delta v_R, \delta P)$ of the form

$$A_1(\omega, m; k_\parallel)\delta v_R + A_2(\omega, m; k_\parallel)\delta v_R' + A_3(\omega, m; k_\parallel)\delta P + A_4(\omega, m; k_\parallel)\delta P' = 0\ . \qquad (9)$$

A prime denotes differentiation with respect to the important R-coordinate, δv_R is again the radial velocity perturbation, and δP denotes the Eulerian total linear pressure (recall that the ratio of these two linear quantities defines the normal acoustic impedance). The coefficients A_i are complex and equilibrium dependent. To derive these equations from the linearized MHD equations, one starts as usual with a Fourier analysis in the ignorable vertical coordinate $\exp(ik_\parallel z)$ and takes advantage of the axisymmetry through Fourier analysis of the azimuthal (angle φ) variation about the fibril as $\exp(im\varphi)$, where m is the integer multipole component. For straight fibrils, the A_i values depend on m^2 only, so that positive and negative values of m cannot be distinguished (this changes if the equilibrium has twist). Also, in these equations, the time dependence is taken as $\exp(-i\omega t)$, but the frequency ω may well be complex. A dimensionless (complex) aspect ratio $ka \equiv a\omega/c_0$ will be used to quantify the frequency. For a fibril of a certain thickness (e.g., one with $k_\parallel a = 0.9$ as will be considered throughout this section), the slow continuum ranges from zero frequency up to $\mathcal{R}e\,(ka) \leq (k_\parallel a)c_{T1}(0)/c_0$, while the Alfvén continuum overlaps the whole slow continuum, but reaches up to higher frequencies, namely, $\mathcal{R}e\,(ka) \leq (k_\parallel a) \times v_{A1}(0)/c_0$. Hence, for general complex frequencies ω (or ka) in the driven problem [time dependence $\exp(-i\omega t)$] of a hot fibril of size $k_\parallel a = 0.9$, we find regimes of (i) both slow and Alfvén resonant absorption, (ii) only Alfvén resonant

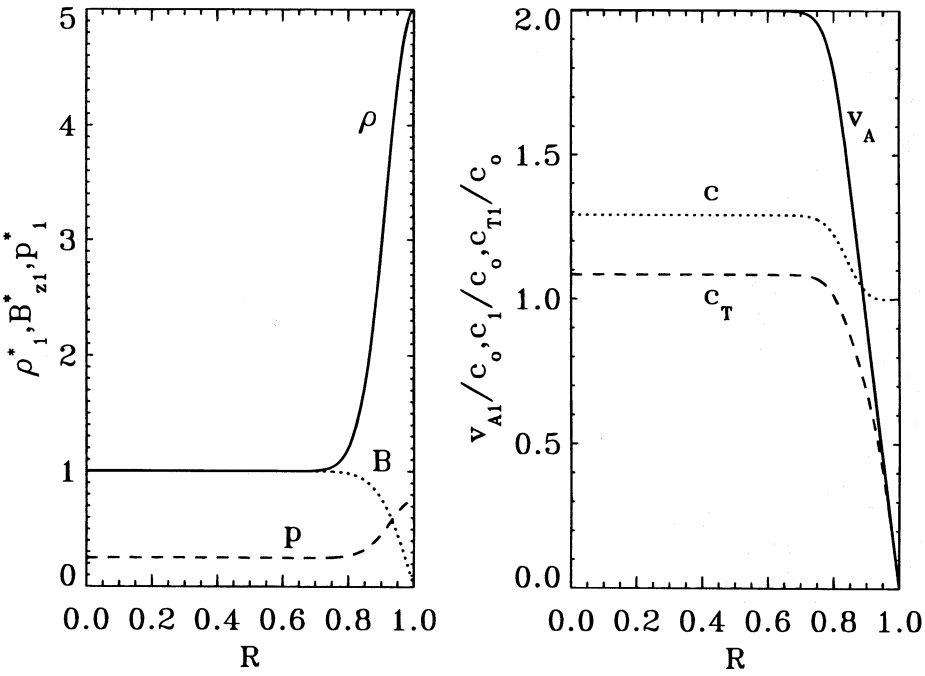

FIG. 1.—*Left*: The radial variation of (dimensionless) density $\rho_1^*(R)$ (*solid line*), magnetic field $B_{z1}^*(R)$ (*dotted line*), and pressure $p_1^*(R)$ (*dashed line*) for a Lou-type equilibrium characterized by a density contrast $D = 5$ and sharpness parameter $\lambda = 75$. *Right*: The corresponding variation of (normalized) Alfvén speed $v_{A1}(R)/c_0$ (*solid line*), sound speed $c_1(R)/c_0$ (*dotted line*) and tube speed $c_{T1}(R)/c_0$ (*dashed line*).

absorption, and (iii) no resonant absorption. Depending on (the real part of) the driving frequency ka, we must incorporate the effects of thin dissipative layers about critical surfaces at which either the local slow or Alfvén frequency is matched (see, e.g., Goossens et al. 1995). This can be done using the so-called connection formulae that link the appropriate Hain & Lüst solutions to the left and right of the dissipative layer(s). Note that when both an Alfvén and a slow resonance occurs, we must make two such connections using the appropriate formulae for the slow and the Alfvén critical surface. Details of this procedure can be found in Sakurai, Goossens, & Hollweg (1991a, 1991b, hereafter SG&Ha, SG&Hb, respectively); novel to our approach is only its use for general complex frequency ω (see also Stenuit, Erdélyi, & Goossens 1995a; Stenuit, Keppens, & Goossens 1995b). In summary, the internal solution for general complex ka, including the effects of Alfvén and/or slow resonances, can be determined from the solution of two (complex) first-order ordinary differential equations in $(\delta v_R, \delta P)$ of the form of equation (9). In principle, we can then calculate the normal acoustic impedance for the transmitted wave field from the boundary values of the solution. Naturally, in practice, the solution must be "tuned" to satisfy boundary conditions, which come into play by a consideration of the external solution.

As far as the outside (unmagnetized) medium is concerned, leakage of acoustic waves from the fibril into this medium may occur for disturbances that have the real part of the aspect ratio $\mathcal{R}e\,(ka) \geq k_{\|}\,a$. For the hot fibrils considered here, this frequency regime of acoustic leakage overlaps partly with the ideal slow and Alfvén frequency continua. Exactly this overlap regime is of interest for the absorption of acoustic power by the fibrils. For a general complex ka, the appropriate solution of the wave equation in the unmagnetized medium can, e.g., be characterized by the normal acoustic impedance for the scattered wave field, Z_{0S} (the additional subscript "0" serves to underline that this impedance is really an external quantity). For this cylindrically symmetric configuration, we define this impedance per multipole component exp $(im\varphi)$. It is constructed from the well-known Hankel function solution to the wave equation external to a cylindrical scatterer (see also the Appendix) as

$$Z_{0S} = \frac{i(ka)}{(k_\perp a)} \frac{H_m^{(1)}(k_\perp a)}{H_m^{(1)\prime}(k_\perp a)} . \tag{10}$$

The symbol $H_m^{(1)}$ denotes the Hankel function of the first kind and order m, and a prime indicates the derivative with respect to its argument. Under this definition, the normal scattered acoustic impedance Z_{0S} is dimensionless (or "specific"), through division by $\rho_0 c_0$. How this expression applies for general complex frequency is hidden within the prescription to calculate the external horizontal wavenumber $k_\perp a$ from the complex aspect ratio ka. To be specific,

$$k_\perp a = \sqrt{(ka)^2 - (k_{\|}\,a)^2} , \tag{11}$$

where we introduce a branch cut on the real axis as $[-k_{\|}\,a, +k_{\|}\,a]$ in the complex ka plane and choose signs for $\mathcal{R}e\,(k_\perp a)$ and $\mathcal{I}m\,(k_\perp a)$ such that $\mathcal{R}e\,[(ka)(\overline{k_\perp a})] \geq 0$ to remove the double-valuedness of the root (the overline means complex conjugate). With the branch cut for the Hankel function of order m running from $-m$ to $-\infty$ along the negative real axis, this implies that for the stable quadrant given by $\mathcal{R}e\,(ka) \geq 0$ and $\mathcal{I}m\,(ka) \leq 0$, the mapping $(ka) \leftrightarrow (k_\perp a)$ is as shown in Figure 2. In particular, the segment $0 \rightarrow +k_{\|}\,a$ of the branch cut itself maps into $ik_{\|}\,a \rightarrow 0$ on the imaginary $k_\perp a$ axis. This ensures that even the nonleaky regime is treated correctly, since under this prescription, the Hankel function ratio in equation (10) with the purely complex argument turns into the appropriate ratio of modified Bessel functions of the second kind. By inspection of equation (10), we note that the scattered acoustic impedance may have poles within the stable quad-

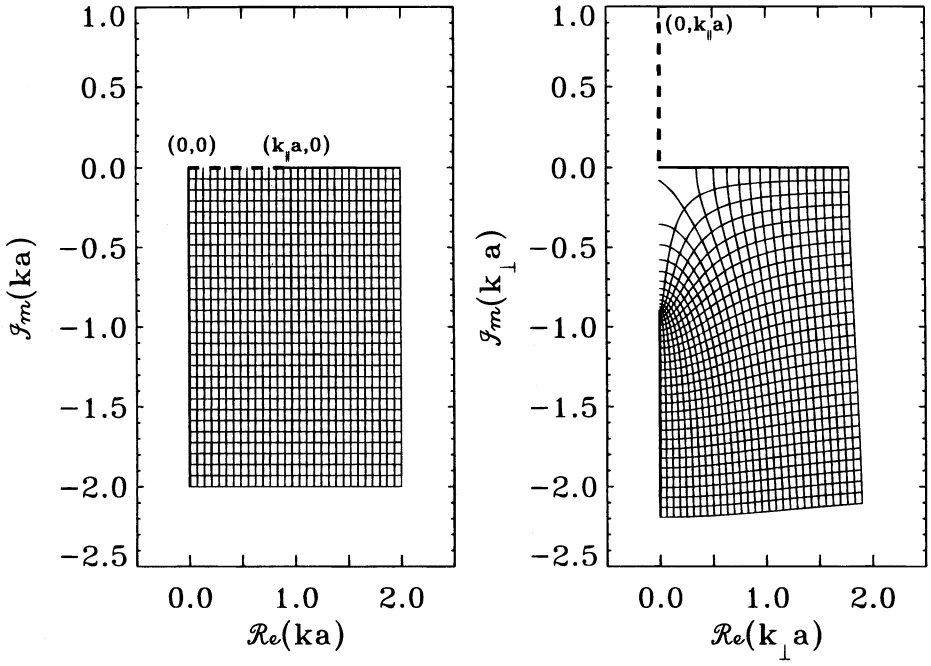

FIG. 2.—The mapping $ka \leftrightarrow k_\perp a$, under the transformation $k_\perp a = [(ka)^2 - (k_{\|}\,a)^2]^{1/2}$ (we took $k_{\|}\,a = 0.9$). Only the stable quadrant $\mathcal{R}e\,(ka) \geq 0$ and $\mathcal{I}m\,(ka) \leq 0$ is shown, and the other quadrants map likewise. Note how the branch cut itself maps onto the imaginary axis in the $k_\perp a$ plane.

rant of the ka plane due to the (complex) zeros of the function $H_m^{(1)\prime}$ in the mapped argument.[4] As a result, these poles largely determine the topology of the real and the imaginary part of the scattered acoustic impedance, regarded as a function of [$\mathcal{R}e\,(ka)$, $\mathcal{I}m\,(ka)$]. Why this realization is important will become clear in the following section.

Other characterizations of the wave field in the uniform surroundings of the cylindrical scatterer are the outgoing normal acoustic impedance, Z_{0O}, which is equal to Z_{0S}; the incoming normal acoustic impedance Z_{0I}, found from Z_{0S} by replacing $H_m^{(1)} \leftrightarrow H_m^{(2)}$; and the exciting normal acoustic impedance Z_{0E}, found from Z_{0S} by replacing $H_m^{(1)} \leftrightarrow J_m$. Here $H_m^{(2)}$ is the Hankel function of the second kind, and the Bessel function is $J_m = (H_m^{(1)} + H_m^{(2)})/2$. We refer to the Appendix and to Keppens (1995b) for the mathematical details.

Now that we have a full characterization of the external solution, and an algorithm to find the internal solution for a general complex aspect ratio ka, we can apply the boundary conditions of continuous total pressure perturbation and continuous normal velocity component at the tube radius a. The net result of applying the boundary conditions for a time dependence exp $(-i\omega t)$ (with ω complex) is to ensure the appropriate amplitude and phase shift for the outgoing and transmitted disturbances, *relative to the incoming disturbance* under the imposed driving exp $(-i\omega t)$ (or equivalently, amplitudes and phase shifts for scattered and transmitted disturbances, relative to the exciting disturbance).

Specifically, for real aspect ratios ka within the range $[k_\parallel a,\ k_\parallel a v_{A1}(0)/c_0]$, a determination of the full solution following the above procedure allows us to investigate the efficiency of the resonant absorption mechanisms. Therefore, we compare the outgoing versus incoming acoustic power by constructing the dimensionless absorption coefficient α_m (defined per multipole; see Appendix as the difference between total incoming versus total outgoing acoustic power, divided by incoming power[5] (see also Braun, Duvall, & Labonte 1987). The result for the hot magnetic fibril mentioned earlier is shown in Figure 3. We plot the monopole ($m = 0$), dipole ($m = 1$), and quadrupole ($m = 2$) absorption coefficients as a function of (real) driving frequency (or ka). Since the equilibrium configuration considered here has no twist, monopole absorption occurs only as long as the frequency lies within the range of the slow continuum, up to $ka \leq 0.976 = (k_\parallel a)c_{T1}(0)/c_0$. However, surprisingly high monopole ($m = 0$) absorption coefficients (up to 43%) are found, given the moderate size of the tube ($k_\parallel a = 0.9$). The absorption coefficients for $m \geq 1$ show a more exotic dependence on frequency:

1. At the lower frequencies $\{ka \in [0.90,\ 0.976] = [k_\parallel a,\ (k_\parallel a)c_{T1}(0)/c_0]\}$, both slow and Alfvén resonant absorption take place but lead to less than 10% dipolar ($m = 1$) absorption and negligible higher order ($m > 1$) absorption coefficients;
2. Above the range of the slow continuum, but within the range of the Alfvén continuum, a series of pronounced absorption maxima accumulates (the resolved peaks are shown in close-up), with absorption coefficients reaching 80% and more;
3. Apart from the afore-mentioned absorption peaks, the Alfvén resonant absorption amounts to less than 20%

[4] The complex zeros of the Hankel function of integer order m (and its derivative) that play a role here lie in the stable half-plane of its argument, near a curve extending from $+m$ to $-m$ and going through $-im \times 0.66274$. See Abramowitz & Stegun (1964).

[5] With this definition for α_m, these absorption coefficients can be calculated easily from the components of the T- or S-matrix for the scatterer: $\alpha_m = 1 - |1 - 2T_m|^2 = 1 - |S_m|^2$. See Appendix.

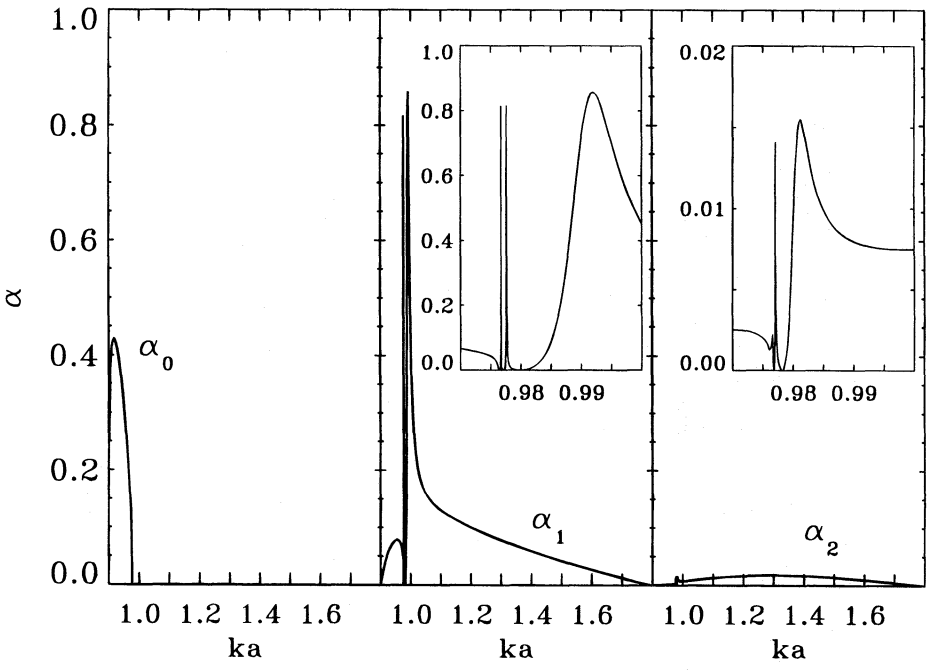

FIG. 3.—The monopole α_0 (*left*), dipole α_1 (*middle*), and quadrupole α_2 (*right*) absorption coefficients as a function of real frequency $ka \equiv \omega a/c_0$, for the equilibrium shown in Fig. 1 and taking the size $k_\parallel a = 0.9$. For dipole and quadrupole, the frequency range immediately above the slow continuum is shown in detail (*insets*). Note the efficient monopolar ($m = 0$) slow resonant absorption, and the absorption maxima in $m \geq 1$ absorption coefficients associated with leaky eigenmodes (§ 2.3).

power loss for the dipole, and negligible higher order ($m > 1$) absorption coefficients.

We emphasize the fact that, in Figure 3, the only place in which both Alfvén and slow resonances occur simultaneously is in the range $ka \in [0.90, 0.976]$, and this only applies for the $m \geq 1$ panels. Clearly, for this equilibrium configuration, the simultaneous occurence of both resonances does not represent a regime of greatly enhanced resonant absorption. However, immediately above the slow continuum, the absorption coefficients found for real driving frequencies reach levels of almost total absorption (up to 80%). Since we have defined complex optimal driving frequencies as those frequencies at which exactly total (100%) absorption takes place, we need to give a more detailed account of the absorption maxima found at real driving frequencies, and their connection with optimal (generally complex) driving frequencies. As these, in turn, are defined from an impedance criterion involving the transmitted normal acoustic impedance Z_T, and this impedance is crucial also for the determination of the leaky eigenmodes, we need also to calculate the complex eigenfrequencies of the fibril embedded in its surroundings.

Once all these connections are clarified, we investigate in § 3 the dependence of the absorption efficiency on the equilibrium parameters (density evacuation D, sharpness λ, and thickness $k_\parallel a$), to assess the relative importance of slow and Alfvén resonant absorption, and the leaky eigenmodes.

2.3. *Leaky Eigenmodes and Optimal Driving Frequencies*

The maxima in the absorption coefficients ($m > 1$) in Figure 3 for the equilibrium shown in Figure 1 can be easily understood: the equilibrium has a uniform "core" throughout approximately 75% of its radius, so that one may expect that the constant tube speed $c_{1T,\mathrm{core}} = c_{1T}(0)$ derived from this uniform core still plays the role of an accumulation point (in complex[!] "phase speed" $\omega/k_\parallel$) of *leaky* eigenmodes. Indeed, were the flux tube uniform throughout, we could calculate analytically the transmitted normal acoustic impedance. To this extent, define a complex internal wavenumber k_1 as

$$(k_1 a)^2 = \frac{[(ka)^2 - (k_\parallel a)^2 v_{A1}^2/c_0^2][(ka)^2 - (k_\parallel a)^2 c_1^2/c_0^2]}{[(ka)^2 - (k_\parallel a)^2 c_{1T}^2/c_0^2][c_1^2/c_0^2 + v_{A1}^2/c_0^2]} . \tag{12}$$

Then the normal acoustic impedance for the transmitted wave field, again scaled to $\rho_0 c_0$, becomes

$$Z_{1T} = \frac{i[(ka)^2 - (k_\parallel a)^2 v_{A1}^2/c_0^2]}{(ka)(k_1 a)} \frac{\rho_1}{\rho_0} \frac{J_m(k_1 a)}{J'_m(k_1 a)} . \tag{13}$$

The particular role played by the tube speed c_{1T} of such a uniform flux tube translates itself in these expressions in the limit $ka \to (k_\parallel a \times c_{1T}/c_0, 0)$ (where ka is in general complex), when the Bessel function ratio J_m/J'_m behaves as a tangent [in fact, in this limit $(J_m/J'_m)(k_1 a) \sim -\cot(k_1 a - m\pi/2 - \pi/4)$], and Z_{1T} has infinitely many, but purely real, poles. Here we regard Z_{1T} as a complex function in the complex argument ka. In what follows, we will demonstrate for the more general case of the flux-tube equilibrium shown in Figure 1, how such poles of Z_{1T} determine the topology of the functions $Z_{0S} - Z_{1T}$ and $Z_{0I} - Z_{1T}$ in argument ka. This, in turn, will allow us to clarify how, from a mathematical point of view, poles of Z_{1T}, leaky eigenmodes (zeros of $Z_{0S} - Z_{1T}$), and optimal driving frequencies (zeros of $Z_{0I} - Z_{1T}$) are ultimately related.

Since for a flux tube with internal radial structure, no analytic result is available for the transmitted wave field,[6] one must resort to a full numerical integration of the Hain & Lüst equation to determine $Z_{1T}(ka)$. As explained in § 2.2, in doing so for a general complex aspect ration ka, we need to take due care when Alfvén and/or slow resonances occur, but this is done consistently using the analytic results of linear dissipative MHD (with the connection formulae from the SG&Ha, SG&Hb prescription, see also Goossens et al. 1995). The complex eigenfrequencies (or aspect ratios ka) for the leaky modes are then found by a determination of

$$\mathcal{K}er\{\mathcal{R}e(Z_{0S} - Z_{1T})(ka)\} \bigcap \mathcal{K}er\{\mathcal{I}m(Z_{0S} - Z_{1T})(ka)\} , \tag{14}$$

where $\mathcal{K}er\{F(z)\}$ stands for the collection of zeros of the function F in argument z. It turns out that the poles of the individual impedances Z_{0S} and Z_{1T} play a dominant role in determining the topology of both functions $\mathcal{R}e(Z_{0S} - Z_{1T}) \equiv \mathcal{R}(\Delta Z)$ and $\mathcal{I}m[Z_{0S} - Z_{1T}] \equiv \mathcal{I}(\Delta Z)$. Therefore, they are a very useful guide in determining the actual zeros of both functions $\mathcal{R}(\Delta Z)$ and $\mathcal{I}(\Delta Z)$. This is best illustrated from Figure 4*a*. To construct Figure 4*a*, we have calculated both functions $\mathcal{R}(\Delta Z)$ and $\mathcal{I}(\Delta Z)$ for the particular hot magnetic fibril of Figure 1 ($k_\parallel a = 0.9$) and Figure 3, taking $m = 0$, in a limited region of the complex ka plane: real and imaginary axes denote the actual portion of the ka plane considered. The heavy solid lines are the sets $\mathcal{K}er\{\mathcal{R}(\Delta Z)(ka)\}$ and $\mathcal{K}er\{\mathcal{I}(\Delta Z)(ka)\}$, as indicated. These are seen to intersect at two complex frequencies, once on the real frequency axis at approximately (0.97897, 0), and once at approximately $(0.97905, -1 \times 10^{-4})$. The dotted and thin solid lines are selected contour lines for negative and positive values of $\mathcal{R}(\Delta Z)$ and $\mathcal{I}(\Delta Z)$, and they serve merely to guide the eye. Since we took $m = 0$, and since the equilibrium considered has straight magnetic field lines (no twist), Alfvén resonant absorption plays no role in Figure 4*a*. Furthermore, in $\mathcal{R}e(ka)$, we are above the slow continuum in Figure 4*a*, so that the only physical mechanism determining the impedances is leakage of acoustic waves into the surroundings. This implies that we may consider equation (13), which is exact for a uniform tube in which only such leakage plays a role, as an approximate expression for the transmitted normal acoustic impedance for the one-dimensional hot magnetic fibril. Then, we must conclude that the crossing of the sets $\mathcal{K}er\{\mathcal{R}(\Delta Z)(ka)\}$ and $\mathcal{K}er\{\mathcal{I}(\Delta Z)(ka)\}$ on the real frequency axis at approximately (0.97897, 0) is *not* a true zero and hence *not an eigenfrequency* of a leaky $m = 0$ sausage mode, but a pole of the transmitted acoustic impedance Z_{1T}. This is recognizable from the behavior of the functions (as suggested by the contour lines) in the vicinity of this pole: the function $\mathcal{I}(\Delta Z)$ behaves singularly along the real frequency (or ka) axis, since the function values tend to plus and to minus infinity on approach of the pole at (0.97897, 0) from opposite ends along the real axis, while the function $\mathcal{R}(\Delta Z)$ likewise behaves singularly but along a direction perpendicular to the real ka axis. This is exactly what the (for our purposes) approximate equation (13) predicts: introducing a large argument expansion for the Bessel

[6] Except for tubes with a thin transition layer: see Keppens (1995b).

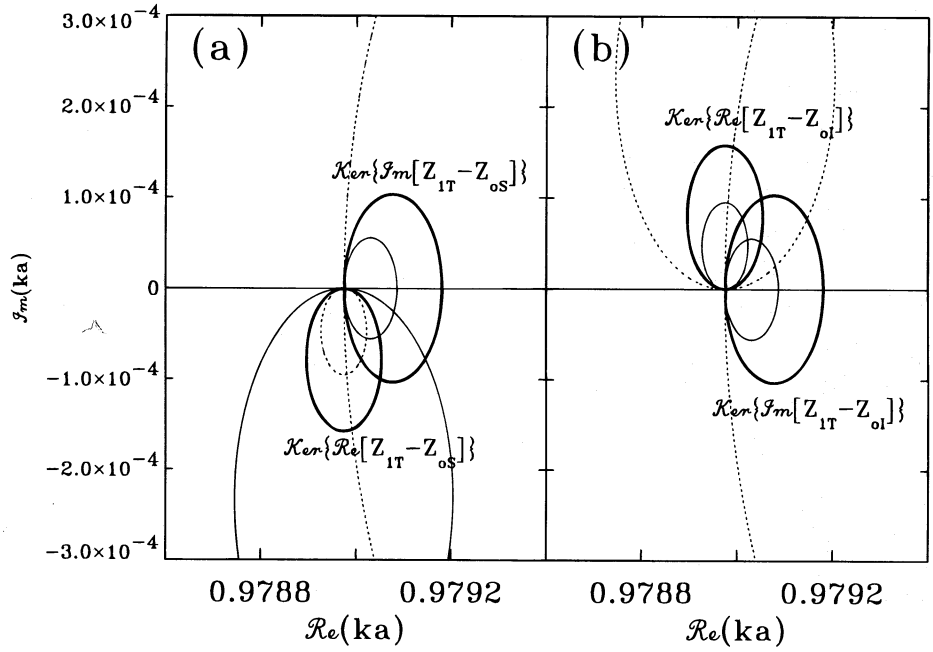

FIG. 4.—How to locate leaky modes and complex optimal driving frequencies from the impedance criteria. This figure applies to the specific equilibrium of Figures 1 and 3 (with $k_\parallel a = 0.9$) and multipole $m = 0$. (*a*) Contour lines of both imaginary and real part of the function $(Z_{1T} - Z_{0S})(ka)$, over a limited region in the complex ka plane. Thick solid lines correspond to zeros of each function, as indicated by $\mathcal{K}er\{\cdot\}$. Thin solid lines and dotted lines are selected contours for positive and negative values, respectively. An absolute zero (or sausage $m = 0$ leaky mode) is found at $ka \approx (0.97905, -1 \times 10^{-4})$, while $ka \approx (0.97897, 0)$ on the real ka axis is a pole of the transmitted normal acoustic impedance Z_{1T}. See text for details. (*b*) Same as (*a*) for the function $(Z_{1T} - Z_{0I})(ka)$. An optimal driving frequency is found at the absolute zero $ka \approx (0.97905, +1 \times 10^{-4})$.

function ratio (for $m = 0$) in Z_{1T} from equation (13) and a small argument expansion (for the sake of argument assuming $k_\perp a$ small) in Z_{0S} of equation (10), the function $\Delta Z(ka)$ is given by

$$\Delta Z \approx i\left[(ka)\ln(k_\perp a) + \overline{(ka)}\,\frac{(ka)^2 - (k_\parallel a)^2 v_{A1}^2/c_0^2}{|ka|^2(k_1 a)} \times \frac{\rho_1}{\rho_0}\cot\left(k_1 a - \frac{\pi}{4}\right)\right]. \quad (15)$$

The presence of the term $\overline{(ka)}$ is then responsible for a (co) tangent-like singularity in $\mathcal{R}(\Delta Z)$ perpendicular to the real ka axis, and in $\mathcal{I}(\Delta Z)$ along the real ka axis, when crossing a pole of Z_{1T}.

As one then approaches the pole throughout the complex plane, and not merely along that unique direction at which the infinities occur, we can understand why the poles are helpful in determining the sets $\mathcal{K}er\{\mathcal{R}(\Delta Z)(ka)\}$ and $\mathcal{K}er\{\mathcal{I}(\Delta Z)(ka)\}$: a pole introduces a *bounded* positive (negative) "island" in an otherwise negative (positive) "landscape" for each function $\mathcal{R}(\Delta Z)(ka)$ and $\mathcal{I}(\Delta Z)(ka)$ separately. Hence, the boundaries of these "islands" constitute the sets $\mathcal{K}er\{\mathcal{R}(\Delta Z)(ka)\}$ and $\mathcal{K}er\{\mathcal{I}(\Delta Z)(ka)\}$. Because of the difference in the directions along which the infinities occur, both "islands" intersect once more, where an absolute zero is found for the impedance difference: a true eigenfrequency of a leaky mode. From Figure 4*a*, we can thus conclude that $ka \approx (0.97905, -1 \times 10^4)$ corresponds to an eigenfrequency of a leaky $m = 0$ sausage mode for the one-dimensional hot magnetic fibril considered.

In summary, the search process to locate the complex eigenfrequencies of leaky modes that we have described above follows from "topological" arguments on both functions $\mathcal{R}(\Delta Z)(ka)$ and $\mathcal{I}(\Delta Z)(ka)$. The poles of the normal acoustic impedances play an essential role in this process, as they determine the sets $\mathcal{K}er\{\mathcal{R}(\Delta Z)(ka)\}$ and $\mathcal{K}er\{\mathcal{I}(\Delta Z)(ka)\}$, which in turn intersect at eigenfrequencies. At this point, it should be stressed that we do not wish to attribute any physical meaning to these poles. In the above process, they merely serve as a tool to determine the physically meaningful leaky eigenmodes![7]

It should be evident that completely analogously, we can locate the optimal driving frequencies that obey the impedance criterion $Z_{0I} = Z_{1T}$. It suffices to replace the Hankel functions of the first kind in equation (10) by Hankel functions of the second kind in the same argument. If we repeat the search process in the vicinity of the pole $ka \approx (0.97897, 0)$ of Z_{1T} for $m = 0$, an optimal $m = 0$ driving frequency is found in the overstable half-plane at $ka \approx (0.97905, +1 \times 10^{-4})$. This is shown in Figure 4*b*. That the optimal driving frequency for $m = 0$ lies in the overstable half-plane is physically consistent, as no $m = 0$ resonant absorption occurs for the frequencies considered. The only possibility to achieve an *apparent* 100% absorption in the linear problem is by driving with an amplitude that grows in time, so that the lag of the amplitude growing of the outgoing wave with respect to the incoming perturbance appears as a total absorption.

While the $m = 0$ case proved to be illustrative, since we could use the approximate expression (13) for frequencies above the slow continuum, it is apparent that in order to explain the behavior of the $m \geq 1$ absorption coefficients in Figure 3, we need to locate leaky modes and optimal driving frequencies for $m \geq 1$. Of course, the same search

[7] Indeed, the function $Z_{0S} - Z_{1T}$ shows up as denominator in the expression for the T-matrix of the cylindrical scatterer (see also eqs. [2] and [3]), and the presence of a similar factor in the numerator and a multiplicative term in front filters out the poles but leaves the zeros of $Z_{0S} - Z_{1T}$ as the physical eigenfrequencies.

pattern can be followed. Again we can concentrate on frequencies immediately above the slow continuum, but now ($m \geq 1$) Alfvén resonant absorption takes place at those frequencies. It should come as no surprise that as a result, the poles of Z_{1T} are no longer on the real frequency axis, but shift into the stable quadrant. An example for $m = 1$ is shown in Figure 5, in the same format as Figure 4. A pole of Z_{1T} is located at approximately $ka \approx (0.987, -0.0014)$, a leaky kink mode is found at $ka \approx (0.9906, -0.0039)$ (Fig. 5*a*), and an optimal driving frequency is $ka \approx (0.9917, -0.0016)$ (Fig. 5*b*). Note that the optimal driving frequency now lies in the stable half-plane. Referring back to Figure 3, we can now attribute the maximum in the absorption coefficient α_1 at real frequency $ka \approx 0.992$ as an immediate consequence of the nearby optimal (but complex) driving frequency.

For the particular one-dimensional hot magnetic fibril from Figures 1 and 3, we summarize our findings in Table 1. Just as for a uniform tube, we find a sequence of leaky eigenmodes for each multipole m: they accumulate toward the top of the slow continuum. In Table 1, only the "higher" frequencies of each sequence are listed. Poles of Z_{1T}, leaky modes, optimal driving frequencies, and real frequencies corresponding to maxima in absorption coefficients (if they exist) are indicated. We repeat that the poles have no physical meaning, but they establish mathematically the connection between leaky eigenmodes and (complex) optimal driving frequencies in a manner explained above. Note in particular that the $m = 0$ mode from Figure 4*a* is the second in a sequence of leaky sausage modes, and that the maxima in the $m \geq 1$ absorption coefficients above the slow continuum (but within the Alfvén frequency range) are closely related to the locations of the leaky modes and the optimal driving frequencies in the complex ka plane (the last digit in each tabulated frequency represents a rounded value; slight differences between the exact frequency of a leaky mode and an optimal driving frequency always occur).

2.4. *Implications for Real Driving Frequencies*

To conclude this section, a critical review of the results of Goossens & Hollweg (1993) is appropriate. These authors have studied the variation of the absorption coefficients as a function of *real* driving frequency, and they were the first to realize the intimate connection with the complex leaky eigenmodes. Our terminology differs from these authors only when referring to optimal driving frequencies: Goossens & Hollweg (1993) define them as those *real* driving frequencies corresponding to the maxima in the absorption coefficients, while we define them as the true, *but in general complex*, driving frequencies at which 100% absorption occurs. Our definition of complex optimal

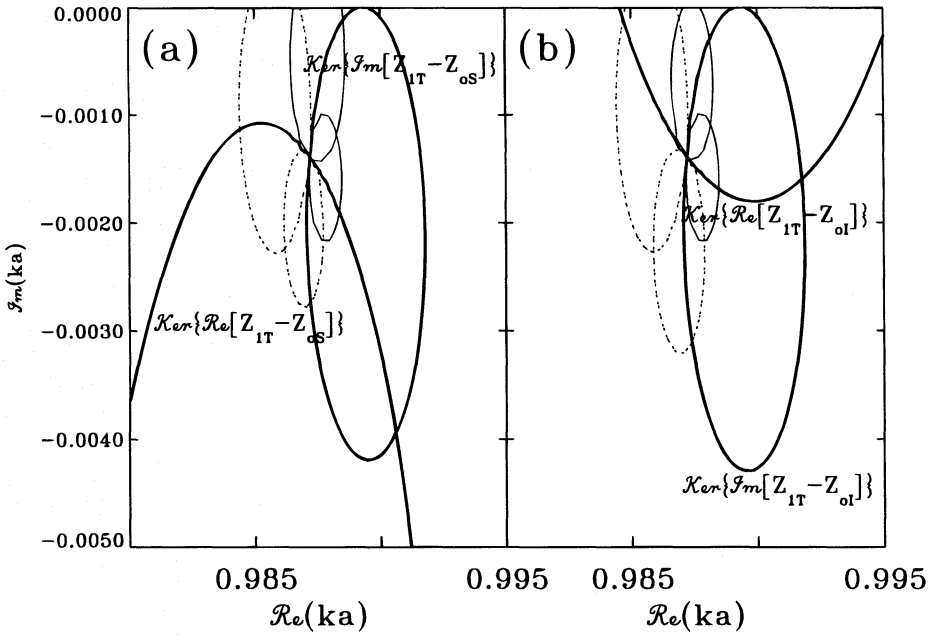

FIG. 5.—Same as Fig. 4, for $m = 1$. A pole of Z_{1T} lies in the stable ka quadrant at $ka \approx (0.987, -1.4 \times 10^{-3})$. From (*a*), a leaky kink mode occurs at $ka \approx (0.9906, -3.9 \times 10^{-3})$. From (*b*), optimal driving corresponds to $ka \approx (0.9917, -1.6 \times 10^{-3})$. Note the connection with the maximum in the absorption coefficient α_1 in Fig. 3 (*middle*) at a real frequency of about $ka \approx 0.992$.

TABLE 1

LOCATION OF POLES, EIGENFREQUENCIES, AND OPTIMAL DRIVING FREQUENCIES IN THE COMPLEX ka PLANE

m	Pole of Z_{1T}	Leaky Mode	100% Absorption	Maximal α_m
0.....	(1.125, 0)	(0.98, −0.115)	(0.98, +0.115)	...
	(0.97897, 0)	(0.97905, -1×10^{-4})	(0.97905, $+1 \times 10^{-4}$)	...
1.....	(0.987, -1.4×10^{-3})	(0.9906, -3.9×10^{-3})	(0.9917, -1.6×10^{-3})	0.992
	(0.97756, -2.1×10^{-5})	(0.977605, -3.6×10^{-5})	(0.977607, -1.55×10^{-5})	0.977607
2.....	(0.9796, -6×10^{-4})	(0.9802, -1.42×10^{-3})	(0.9802, -1.42×10^{-3})	0.981
	(0.97701, -3×10^{-5})	(0.97704, -4.5×10^{-5})	(0.97704, -4.5×10^{-5})	0.97705

driving frequencies is derived from physical principles, as we have obtained an impedance criterion for optimal driving, analogous to the impedance criterion satisfied by the leaky eigenmodes. Naturally, equilibria may exist where one (or perhaps several) of the (generally complex) optimal driving frequencies satisfying $Z_{0I} = Z_{1T}$ lie *on the real frequency axis*, so that *total* absorption takes place at a particular *real* frequency. Thus, it follows that Goossens & Hollweg (1993) concluded correctly that *total* absorption at a *real* optimal driving frequency takes place only when the equilibrium is fine tuned with respect to the incoming wave. Likewise, Goossens & Hollweg (1993) were correct to point out that a condition for total absorption can be interpreted as an impedance criterion. A subtle correction to their results concerns the realization that one can always define complex optimal driving frequencies for which $\alpha = 100\%$ from the impedance criterion $Z_{0I} = Z_{1T}$. Therefore, the condition for total absorption is not merely an impedance matching on both damping mechanisms (acoustic leakage and resonant absorption), as explained by Goossens & Hollweg (1993): the complex impedances Z_{0I} and Z_{1T} actually have both a real and an imaginary part, commonly referred to as resistance and reactance, respectively. Total absorption requires the simultaneous equality of resistances (related to damping) and reactances. The reason why Goossens & Hollweg (1993) concluded only on the impedance matching for both damping mechanisms as a condition for total absorption at a real optimal driving frequency is understood as follows. Their results derive from Taylor expansions in real frequencies about the real part of the complex eigenfrequency of a leaky mode. Now, the complex eigenfrequency of a leaky mode satisfies $Z_{0S} = Z_{1T}$ (or $Z_{0O} = Z_{1T}$, since $Z_{0O} = Z_{0S}$), so that both resistances and reactances of scattered and transmitted field are equal. Further, the differences $Z_{0S} - Z_{0I}$ for real frequencies is purely real (which follows easily from eq. [10]), so that the reactances for scattered and incoming field are always equal for real frequencies. If we then Taylor expand from the real part of the eigenfrequency of a leaky mode to find a condition for total absorption at a real driving frequency, we satisfy automatically the condition of equal reactances for incoming and transmitted wave field, so that we are left with the condition on equal resistances.

Under most conditions, the difference $Z_{0S} - Z_{0I}$ is small, which is why leaky modes, optimal driving frequencies, and the real driving frequencies corresponding to maxima in the absorption coefficients are all connected (see Table 1). However, it should be clear that our definition of complex optimal driving frequencies is more general and holds even when leaky eigenmodes and optimal driving frequencies are separated by sufficient amounts requiring higher than first-order Taylor expansions (note in particular the case $m = 0$ in Table 1). Therefore, our results confirm, but also extend, the results obtained by Goossens & Hollweg (1993).

3. VARIATIONS IN THE EQUILIBRIUM PARAMETERS

With the connection between leaky eigenmodes, complex optimal driving frequencies, and maxima in the absorption coefficients as a function of real driving frequency spelled out in detail (see Table 1) for the particular fibril with $D = 5$, $\lambda = 75$, and $k_{\|} a = 0.9$, we may ask how the equilibrium structure plays a role in the efficiency of the resonant absorption. After all, although the equilibrium of Figure 1 proved useful to demonstrate these connections, a density contrast of $D = 5$ may seem quite large to model a magnetic element, and more critically, the temperature contrast was too high. Likewise, it may be of interest to know what happens if the equilibrium varies more gradual throughout the tube (measured by λ), and what changes if the tube is bigger. In the opposite limit of a thin tube with a thin transition layer, the analytic results of Keppens (1995b) are appropriate, so that we can restrict the parameter variations to decreasing the density contrast D, increasing the transition layer by decreasing λ, and exploring what happens for larger $k_{\|} a$.

When the density contrast D is lowered, at fixed sharpness $\lambda = 75$ and thickness $k_{\|} a$, both the Alfvén and slow frequency ranges shift to lower frequencies. This is seen easily from equation (8), since that part of the Alfvén and slow continuum of interest for resonant absorption is $[k_{\|} a, (k_{\|} a) v_{A1}(0)/c_0]$ and $[k_{\|} a, (k_{\|} a) c_{T1}(0)/c_0]$, respectively. We note that our one-dimensional "model" for a magnetic element based on equations (4)–(6), with a value of the sharpness parameter $\lambda = 75$, is quite consistent with a transition layer of about 10% in radius for magnetic elements (see Knölker, Schüssler, & Weisshaar 1988), as can be seen from the variation of $c_1(R)/c_0$ in Figure 1. The shift to lower frequencies of the slow continuum with decreasing D is such that, as soon as the density contrast D drops below about 4.25, the slow continuum is no longer accessible for acoustic excitation. Therefore, to determine whether the slow continuum plays any (significant) role in a "realistic" magnetic element, we can deduce the dimensionless appropriate parameter values (density contrast D; characteristic speed ratios v_{A1}/c_0, c_1/c_0, c_{T1}/c_0; and tube thickness as measured by $k_{\|} a$) from semiempirical determinations of the vertical internal structure of magnetic elements (Keller et al. 1990) with respect to a reference nonmagnetic atmosphere model (VAL + Spruit model; Vernazza, Avrett, & Loeser 1976, Spruit 1977). As our calculations are only one-dimensional, we need these quantities (D, $k_{\|} a$, etc.) as a function of equal geometrical height (not equal optical depth!) when comparing the internal versus the external quantities. This is shown in Figure 6, for both a plage (*left panel*) and a network (*right panel*) magnetic element.[8] The zero level of geometrical height z corresponds to the level of continuum formation in the nonmagnetic atmosphere. It is important to note that in these models, the *assumed* values for the continuum contrast on the axis of the flux tubes are 1.3 for the plage and 1.4 for the network flux tube. The network magnetic element is therefore somewhat hotter than the plage element, and both are hotter than the surrounding atmosphere at heights greater than 200 km (where $c_1/c_0 > 1$ [*lower dotted lines*]; a solid line delineates $c_1 = c_0$). The thickness of the tube $k_{\|} a$ (*dashed line*) is deduced from a flux conservation argument and set arbitrarily at 300 km diameter ($2a$) at $z = 0$, with a heuristic value of $k_{\|} \approx 2 \times 10^{-3}$ km^{-1} for p-modes in the solar photospheric layers. As noted by Keller et al. (1990) and evidenced by the virtually identical flaring of the plage and network magnetic element with height in Figure 6 (*dashed line* in both panels), the magnetic structure of both

[8] This figure is produced from the results of Keller et al. (1990). These authors note that these models are most reliable in the layer extending from about −100 km (roughly the Wilson depression for these structures) up to +300 km.

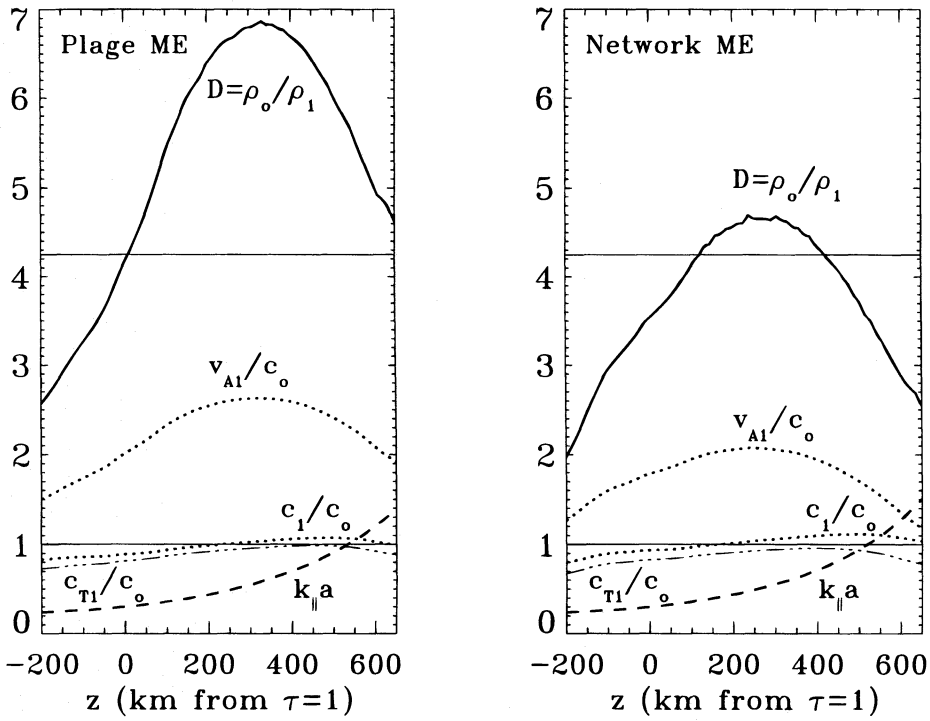

FIG. 6.—Vertical equilibrium structure for plage (*left*) and network (*right*) flux tubes compared vs. a nonmagnetic reference atmosphere as a function of geometrical height (z in km above photospheric $\tau = 1$), produced from the semiempirical results by Keller et al. (1990). Thick solid lines indicate the density contrast D; dotted lines are used for the speed ratios v_{A1}/c_0 and c_1/c_0. Dashed line indicates $k_\parallel a$ deducted from flux conservation (see text), and the tube speed is indicated as a dash-dotted line.

kinds of flux tubes is comparable, but the network tube has a slightly lower field strength than the plage tube (1550 G for the network tube at $z = 0$ vs. 1610 G for the plage tube). From Figure 6, it can be seen that both plage and network flux tubes reach high levels of evacuation D (*solid lines* in both panels) in the higher photospheric layers: a horizontal solid line delineates the level $D = 4.25$ mentioned above. The run of the normalized tube speed c_{T1}/c_0 for both flux tube models is given by the dash-dotted lines. As the tube speed nears (but never quite exceeds) the external sound speed (especially in the plage element) at a height of about 400 km above photospheric $\tau = 1$, we suggest that in those higher photospheric layers, the slow continuum and the associated eigenmodes for hot evacuated magnetic fibrils may play a role in the interaction of waves with the fibrils. Note also that in those higher layers, the tubes have reached dimensions of the appropriate order $k_\parallel a \propto O(1)$, due to flaring. However, we emphasize that firm conclusions cannot be drawn as based on an *oversimplified* one-dimensional hot magnetic fibril model, and that the dynamic nature of real magnetic elements may not validate a comparison with a static model atmosphere as suggested by Figure 6. In any case, it is clear that in the lower photospheric layers, in which $k_\parallel a$ drops to about 0.3 (and lower) and the density contrast lies considerably below 4.25, neither the slow continuum nor the associated eigenmodes play a role. In fact, for a one-dimensional "magnetic element" at those layers modeled by $D = 3.25$, $\lambda = 75$, and $k_\parallel a \approx 0.25$, only a negligible amount of Alfvén resonant absorption takes place, with the largest absorption coefficient α_m obtained for $m = 1$ (dipole), but at a value typically less than 1% (see also Keppens 1995a, 1995b).

If we keep the density contrast $D = 5$ and decrease instead the sharpness parameter λ while keeping the size fixed at $k_\parallel a = 0.9$, the absorption coefficients change as indicated in Figure 7. We decreased λ by one order of magnitude, from $\lambda = 75$ through $\lambda = 7$. The intermediate value $\lambda = 35$ corresponds to an equilibrium at which the transition layer is about 50% in radius, while at $\lambda = 7$, the variation of the equilibrium quantities is smooth throughout. The left panel of Figure 7 shows the monopole absorption coefficient α_0, which is due entirely to slow resonant absorption (the equilibrium has straight field lines). Hence, $\alpha_0 = 0$ at frequencies above $ka = (k_\parallel a)c_{1T}(0)/c_0 \approx 0.976$. Note how the slow $m = 0$ resonant absorption becomes increasingly important (with monopole absorption coefficients eventually up to more than 80% over the whole extent of the slow continuum) when the radial equilibrium variation becomes more gradual. This is true, even though the tube is quite thin: we kept the size fixed at $k_\parallel a = 0.9$. Monopolar ($m = 0$) slow resonant absorption is thus surprisingly efficient under certain equilibrium conditions.

The right panel of Figure 7 shows the dipole absorption coefficient α_1. We have filtered out the frequency range immediately above the slow continuum at which the absorption maxima were found to accumulate (for $\lambda = 75$; see Fig. 3). Below $ka \approx 0.976$, combined slow and Alfvén resonant absorption takes place but leads to modest dipole absorption coefficients $\alpha_1 \leq 12\%$ for all sharpness parameters λ shown. Within the frequency range in which only Alfvén resonant absorption occurs, we find typically $\alpha_1 \leq 15\%$. It appears that for a fibril of fixed density contrast and size $ka \approx O(1)$, the variation of the equilibrium quantities has no dramatic effects on its $m \geq 1$ absorption properties.

Figure 8 shows how for larger tubes, still characterized by $D = 5$ and $\lambda = 75$, the absorption coefficient maxima shift in frequency away from the tip of the slow continuum and broaden within the range of the Alfvén continuum. We

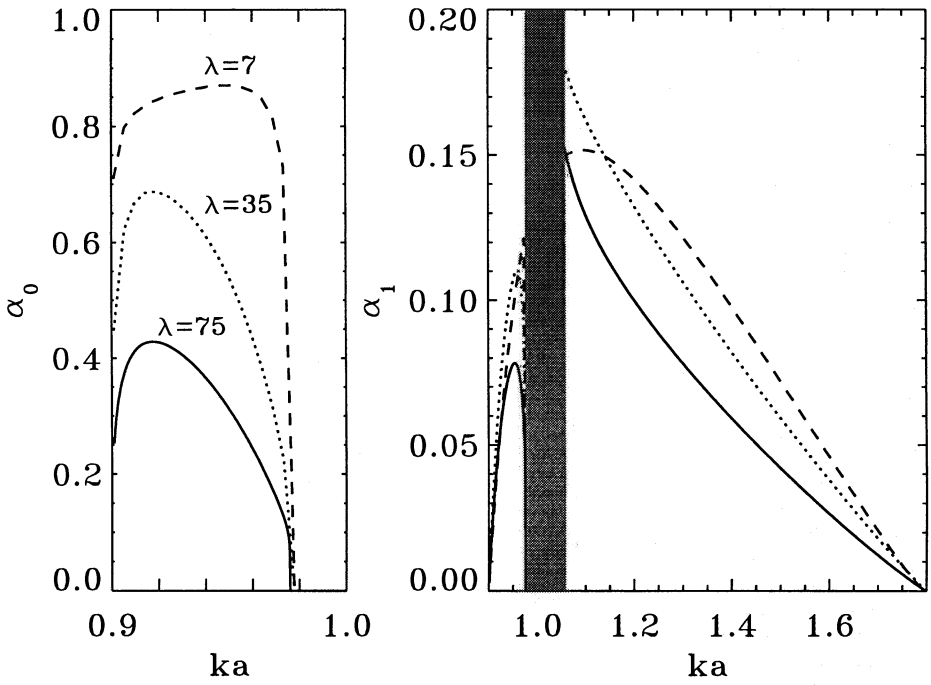

FIG. 7.—Monopole α_0 (*left*) and dipole α_1 (*right*) absorption coefficient as a function of real driving frequency ka, for hot fibrils of size $k_\parallel a = 0.9$ and density contrast $D = 5$, varying the sharpness λ through 75 (*solid line*, as in Fig. 3), 35 (*dotted line*), and 7 (*dashed line*). Note the scale difference in the abscissa: for the monopole, we zoomed in on the slow continuum. Smoother equilibria have surprisingly large monopole absorption coefficients. For $m = 1$, the frequency range in which peaks occur is filtered out artificially (*shaded region*).

increased $k_\parallel a$ through (0.9, 2, 3) and plotted the dipole (*left*) and quadrupole (*right*) absorption coefficients as a function of $k/k_\parallel$. For the given parameters D and λ, this means that the slow continuum reaches up to $k/k_\parallel \approx 1.085$, while the Alfvén frequencies reach up to $k/k_\parallel \approx 2$: therefore, note the abscissa range in Figure 8. Figure 8 suggests that the sequences of leaky modes and optimal driving frequencies (one sequence for each multipole index m) found at the tip of the slow continuum may eventually dominate the absorption properties of larger hot and evacuated magnetic flux tubes. This is particularly apparent in the quadrupole (α_2) absorption coefficient.

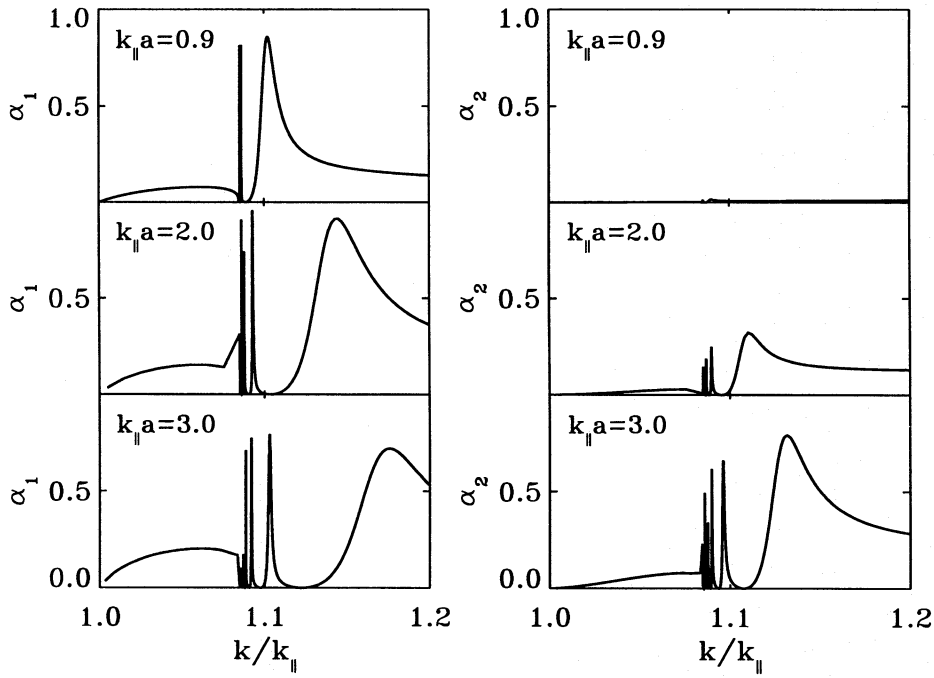

FIG. 8.—Dipole α_1 (*left*) and quadrupole $m = 2$ (*right*) absorption coefficients as a function of (real) $k/k_\parallel$ for hot fibrils with $D = 5$, $\lambda = 75$ (as in Fig. 1), of sizes $k_\parallel a = 0.9$, 2, and 3 (as indicated). The absorption maxima shift to higher frequencies and start to dominate the absorption throughout the Alfvén continuum when the size of the fibrils increases.

4. CONCLUSIONS

The results of this paper may be summarized as follows.

Introducing normal acoustic impedances, we were able to derive impedance criteria for both eigenmodes and optimal driving frequencies for completely general cylindrical scatterers. Complex frequencies at which scattered (or outgoing, since $Z_S = Z_O$) and transmitted normal acoustic impedances are equal correspond to eigenmodes (see also Keppens 1995b), and complex frequencies at which incoming and transmitted normal acoustic impedances are equal are optimal in the sense that (apparent) 100% absorption occurs. Since the transmitted normal acoustic impedance appears in both criteria, eigenmodes and optimal driving frequencies are ultimately connected.

In the context of linear MHD, these impedance criteria prove extremely useful to obtain a full understanding of the efficiency of both slow and Alfvén resonant absorption for flux tubes embedded in wave-carrying surroundings. In § 2, we presented an illustrative calculation of complex leaky modes, complex optimal driving frequencies, and the run of the absorption coefficients for different multipoles m as a function of real driving frequencies for a so-called hot magnetic fibril with nonnegligible radial structure. We choose to give a detailed account of the search process followed to find leaky modes and optimal frequencies from the complex impedance criteria that they satisfy: one must take due care when dealing with general complex frequencies ω in $\exp(-i\omega t)$. For the one-dimensional hot magnetic fibril embedded in unmagnetized homogeneous surroundings, we were able to treat simultaneously both slow and Alfvén resonant absorption, and the possibility for acoustic leakage into the surroundings, and this for general complex frequencies. Wherever possible, analytic results were used in the interpretation, but it is realized that for the one-dimensional fibrils considered, numerical techniques must be exploited. To deal with the resonant absorption, the SG&Ha, SG&Hb prescription was implemented (as in Stenuit et al. 1995a). Together with a numerical integration of the Hain & Lüst (1958) equation and the analytic results pertinent to the external homogeneous medium, a complete description was possible. The results of Keppens (1995b) extend the results presented here analytically, since for flux tubes with a thin transition layer there is no need for a numerical integration of the Hain & Lüst equation.

We found that a one-dimensional hot and evacuated magnetic fibril of size $k_{\|} a \approx 1$ is an efficient monopole ($m = 0$) absorber of incident acoustic power, as long as the slow continuum can be accessed. This efficiency of the monopolar slow resonant absorption is even more pronounced for smoother equilibrium profiles. Moreover, sequences of leaky modes and optimal driving frequencies accumulate toward the top of the slow continuum, giving rise to maxima in the run of absorption coefficients as a function of real frequency within the Alfvén continuum, at the transition out of the slow continuum. These maxima in the absorption coefficients as a function of real driving frequency are related directly to the near presence of a complex optimal driving frequency close to the real frequency axis in the stable complex frequency half-plane. Through the impedance criteria, each optimal driving frequency seems related to a leaky eigenmode of the fibril in its infinite surroundings (Table 1). Further, these sequences of discrete leaky modes and optimal driving frequencies may start to dominate the absorption properties of larger hot and evacuated flux tubes with internal radial structure.

Within the solar context, we suggest that the slow continuum and the associated eigenmodes may play a role in the absorption and scattering properties of the hot and strongly magnetized (kG) magnetic elements at higher photospheric layers (typically 400 km above the level of continuum formation). In the lower photospheric layers, their evacuation is simply not large enough to make the slow continuum accessible, and their diameters (200–300 km) are too small to achieve a sufficient amount of resonant absorption.

In addition, we could reevaluate the results obtained by Goossens & Hollweg (1993). These authors realized the connection between leaky eigenmodes and the maxima in the absorption coefficients as a function of real driving frequency. Our results called for a subtle change in their nomenclature: the optimal driving frequencies are in general *complex* and are best defined from the impedance criterion $Z_{0I} = Z_{1T}$. This in turn confirms that the equilibrium must be fine tuned to the incoming wave in order to achieve total absorption at a *real* driving frequency. Naturally, our definition of optimal driving frequencies includes the possibility of the physically uninteresting optimal driving frequencies with an exponentially growing amplitude (imaginary part $\omega_I > 0$), such that only apparent total absorption occurs. For real driving frequencies, the optimal driving frequencies on the real frequency axis, or close to the real frequency axis, but in the stable complex half-plane, are of primary physical importance.

Finally, we called for similar investigation of the close connection between the slow continuum, the complex leaky modes, the optimal driving frequencies, etc., in twisted flux-tube equilibria. The presence of twist in the (axisymmetric) equilibrium decouples the slow continua corresponding to different multipole components m, and this may be important when studying their absorption and scattering properties. This will be addressed in a forthcoming paper (Stenuit et al. 1995b).

This work has been inspired by earlier collaborations in the context of linear MHD; I thank T. J. Bogdan and Professor M. Goossens for passing on their knowledge in this field. I wish to thank Hilde Stenuit for reading and commenting on the manuscript, and M. Schüssler for supplying me with the reference flux tube atmospheres of Figure 6. I thank an anonymous referee for helpful suggestions and a critical assessment of the original manuscript.

APPENDIX

A NOTE ON IMPEDANCES

In this Appendix, we collect some of the basic ideas set forth in Keppens (1995b) on normal acoustic impedances and their importance in linear MHD problems. A starting point, suitable for the problem at hand, is to obtain an analytic expression

for the wave field in the uniform, but unmagnetized, surroundings of a cylindrically symmetric, longitudinally invariant cylindrical scatterer of radius a (which does not need to be specified further). This boils down to solving the wave equation in the infinite, but uniform, region (sound speed c_0) external to a cylinder, and after Fourier analyzing as exp ($ik_\parallel z$) exp ($im\varphi$) exp ($-i\omega t$), we find for the radial dependence (R-coordinate) of the linear velocity potential ϕ defined from $\delta \boldsymbol{v} = -\nabla\phi$ (such that the linear pressure is given by $\delta p = -i\omega p_0 \phi$, with ρ_0 the uniform external equilibrium density) the following solution:

$$\phi_{\omega k_\parallel m}(R) = \alpha_{\rm in}(\omega; k_\parallel, m) H_m^{(2)}(k_\perp R) + \alpha_{\rm out}(\omega; k_\parallel, m) H_m^{(1)}(k_\perp R)\,, \tag{16}$$

where $k_\perp$ is the component of the wavevector perpendicular to the cylinder axis. Through the dispersion relation of the uniform medium $k^2 c_0^2 = \omega^2$, we have that $k_\perp^2 = k^2 - k_\parallel^2$. This way of writing the external solution by means of Hankel functions of the second ($H_m^{(2)}$) and first ($H_m^{(1)}$) kind and order m decomposes the wave field external to the cylinder in incoming and outgoing cylindrical waves, essentially. The complex coefficients ($\alpha_{\rm in}$, $\alpha_{\rm out}$) give amplitudes and phases to the incoming and outgoing waves. We construct a complex number T_m (a component of the so-called T-matrix) per multipole exp ($im\varphi$), from these complex coefficients as

$$T_m(\omega; k_\parallel) = \frac{1}{2}\left[1 - \frac{\alpha_{\rm out}(\omega; k_\parallel, m)}{\alpha_{\rm in}(\omega; k_\parallel, m)}\right]. \tag{17}$$

If we then consider the amplitude of the outgoing wave, relative to the amplitude of the incoming wave, i.e., make the ratio $|\alpha_{\rm out}/\alpha_{\rm in}|$, and also calculate the relative phase shift $\delta_m = \mathrm{Arg}\,(\alpha_{\rm out}) - \mathrm{Arg}\,(\alpha_{\rm in})$ ("Arg" for argument), we may write

$$T_m = \tfrac{1}{2}(1 - \sqrt{1 - \alpha_m}\, e^{-i\delta_m})\,,$$

where $\alpha_m = 1 - |\alpha_{\rm out}/\alpha_{\rm in}|^2$ is the absorption coefficient for the mth multipole (see, e.g., Braun et al. 1987). This absorption coefficient is a measure of the power absorbed out of the incoming wave field by the scatterer.

So far, we have not said anything explicitly about the scatterer and the transmitted wave field. However, it is clear that while we may prescribe the incoming wave field by choosing $\alpha_{\rm in}$, the scatterer will impose the relative amplitude and phase shifts of the outgoing wave, hence $\alpha_{\rm out}$. It does so in accord with the boundary conditions valid at its radius a, namely, by keeping the total linear pressure perturbation δP continuous across its circumference, and by keeping the normal velocity component δv_R continuous (no vacuum should form). In terms of a description of the external wave field in incoming and outgoing waves (as above), this means that at radius a, we have $\delta P_{\rm tr} = \delta p_{\rm in} + \delta p_{\rm out}$ and $\delta v_{R,{\rm tr}} = \delta v_{R,{\rm in}} + \delta v_{R,{\rm out}}$, where the subscript "tr" stands for the transmitted wave field and a δP is used for the internal total linear pressure (which may have a part from, e.g., magnetic pressure), and δp is the external linear (gas) pressure. Defining impedances Z for each of the wave field components (transmitted, incoming, and outgoing), and per multipole component exp ($im\varphi$), as the ratio of linear pressure to normal velocity, one can manipulate these conditions valid at radius a, to eliminate the unknown amplitude $\alpha_{\rm out}$. To do so, we denote impedances as Z_T, Z_I, and Z_O for the transmitted, incoming, and outgoing wave fields, respectively, and we start from the boundary conditions to write the identity

$$1 - 2T_m = \frac{v_{R,{\rm in}}}{v_{R,{\rm out}}/(1 - 2T_m)}\left(\frac{Z_T - Z_I}{Z_O - Z_T}\right). \tag{18}$$

This expression (which is our eq. [3]) tells us that $1 - 2T_m = 0$, or $\alpha_m = 1$, when $Z_T = Z_I$. Physically, this means that we have 100% absorption, or no outgoing wave, when the impedance criterion $Z_T = Z_I$ is fulfilled. It tells us also that the poles of the T-matrix element T_m correspond to the impedance criterion $Z_O = Z_T$. Returning to the defining expression (17), the poles of T_m correspond to $\alpha_{\rm in} = 0$, or no incoming wave. This means that these poles, found from $Z_O = Z_T$, give the physical eigenfrequencies of the scatterer, where no imposed incoming wave is present.

To derive our equation (2) in an analogous manner, a similar elimination process rewrites $\alpha_{\rm out} = \alpha_{\rm in}(1 - 2T_m)$ (the definition of T_m) and eliminates T_m. This turns out to be equivalent to writing the solution of the wave equation external to the cylinder in its exciting and its scattered part, instead of decomposing it in incoming and outgoing waves. The exciting part is that part of the external wave field associated with the Bessel function $J_m = (H_m^{(1)} + H_m^{(2)})/2$, while the scattered part is the part due entirely to the presence of the scatterer itself. Going through the algebra, this yields a normal acoustic impedance Z_S for the scattered wave field that is identical to the outgoing one Z_O. For more details, we refer to Keppens (1995a, 1995b).

REFERENCES

Abramowitz, M., & Stegun, I. A. 1964, Handbook of Mathematical Functions with Formulas, Graphs, and Mathematical Tables (Washington, DC: National Bureau of Standards)
Braun, D. C., Duvall, T. L., Jr., & LaBonte, B. J. 1987, ApJ, 319, L27
Cally, P. S. 1986, Sol. Phys., 103, 277
Defouw, R. J. 1976, ApJ, 209, 266
Goedbloed, J. P. 1983, Lecture Notes on Ideal Magnetohydrodynamics (Rijnhuizen Rep. 83-145, Association Euratom)
Goossens, M., & Hollweg, J. V. 1993, Sol. Phys., 145, 19
Goossens, M., & Poedts, S. 1992, ApJ, 384, 348
Goossens, M., Ruderman, M. S., & Hollweg, J. V. 1995, Sol. Phys., 157, 75
Hain, K., & Lüst, R. 1958, Z. Naturforsch. 13a, 936
Hollweg, J. V. 1988, ApJ, 335, 1005
Keller, C. U. 1992, Nature, 359, 307
Keller, C. U., Solanki, S. K., Steiner, O., & Stenflo, J. O. 1990, A&A, 233, 583
Keppens, R. 1995a, Ph.D. thesis, Katholieke Univ. Leuven
———. 1995b, Sol. Phys. 161, 251
Knölker, M., Schüssler, M., & Weisshaar, E. 1988, A&A, 194, 257
Lou, Y. Q. 1990, ApJ, 350, 452
Morse, P. M., & Feshbach, H. 1953, Methods of Theoretical Physics (New York: McGraw-Hill)
Poedts, S., Goossens, M., & Kerner, W. 1989, Sol. Phys., 123, 83
———. 1990, ApJ, 360, 279
Sakurai, T., Goossens, M., & Hollweg, J. V. 1991a, Sol. Phys., 133, 227 (SG&Ha)
———. 1991b, Sol. Phys., 133, 247 (SG&Hb)
Schüssler, M. 1991, Geophys. Astrophys. Fluid Dyn., 62, 271
Solanki, S. 1993, Space Sci. Rev., 63, 1
Steiner, O., Grossmann-Doerth, U., Knölker, M., & Schüssler, M. 1996, in Reviews in Modern Astronomy, Vol. 8, ed. G. Klare (Hamburg: Astronomische Gesellschaft), in press
Stenuit, H., Erdélyi, R., & Goossens, M. 1995a, Sol. Phys., 161, 139
Stenuit, H., Keppens, R., & Goossens, M. 1995b, in preparation
Spruit, H. C. 1977, Ph.D. dissertation, Univ. Utrecht
———. 1982, Sol. Phys., 75, 3
Vernazza, J. E., Avrett, E. H., & Loeser, R. 1976, ApJS, 30, 1
Wilson, P. R. 1981, ApJ, 251, 756